Supplement of Geosci. Model Dev., 18, 6623–6645, 2025
https://doi.org/10.5194/gmd-18-6623-2025-supplement


Geoscientific Model Development
Open Access
EGU

*Supplement of*

# Implementing a process-based representation of soil water movement in a second-generation dynamic vegetation model: application to dryland ecosystems (LPJ-GUESS-RE v1.0)

**Wim Verbruggen et al.**

*Correspondence to:* Wim Verbruggen (wim.verbruggen@bio.ku.dk)

## S1 Hydrological processes and parameters in LPJ-GUESS v4.1

This section contains an overview of plant transpiration processes and the pedotransfer functions used to calculate soil hydraulic parameters and properties, both shared between the default and RE-based versions of the LPJ-GUESS v4.1 model.

### S1.1 Pedotransfer functions

We slightly modified the pedotransfer functions (PTF) in order to calculate water potentials as negative values with units of meter of head (m). The default version of the model uses positive values with units of meter of head (m). We used the updated PTFs for both the default and the updated model versions throughout the manuscript. The model often converts between units of pressure (MPa) and meter of head by the following conversion factor:

$$MPa2m = 102.2435\ m/MPa$$

The four shape parameters used by the Campbell (1974) relations are calculated based on the empirical formulae derived by Cosby et al. (1984) and used in the model in the formulations given below, where *sand* and *clay* represent the fractions of sand and clay in the soil:

Soil matric potential at saturation $\psi_s$ (units: $m$)

$$\psi_s = -0.01 * 10^{2.17-1.58*sand-0.63*clay} \quad (1)$$

Soil water content at saturation $\theta_s$ (units: $m^3/m^3$)

$$\theta_s = 0.01 * 10^{50.5-14.2*sand-3.7*clay} \quad (2)$$

Hydraulic conductivity at saturation $K_s$ (units: $m/s$)

$$K_s = 6.817 * 10^{-6.6+1.26*sand-0.64*clay} \quad (3)$$

The shape parameter ($b$) which describes the slope of the soil water retention curve:

$$b = 3.10 + 15.7 * clay - 0.3 * sand \quad (4)$$

The wilting point is defined at the soil matric potential of

$$\psi_{wp} = -1.5\ MPa \tag{5}$$

$$\theta_{wp} = \theta_s \left(\frac{\psi_{wp}}{\psi_s}\right)^{-\frac{1}{b}} \tag{6}$$

For calculating soil moisture and water potential at field capacity, we use the formulation by (Romano and Santini, 2002) who define that soil reaches field capacity when $K = 0.1\ mm/d = 1.157407 * 10^{-9}\ m/s$, leading to:

$$\theta_{fc} = \theta_s \left(\frac{1.157407 * 10^{-9}}{K_s}\right)^{\frac{1}{2b+3}} \tag{7}$$

$$\psi_{fc} = \psi_s \left(\theta_{fc}/\theta_s\right)^{-b} \tag{8}$$

Plant-available soil water capacity $\theta_{awc}$ is defined as the difference between $\theta_{fc}$ and $\theta_{wp}$ :

$$\theta_{awc} = \theta_{fc} - \theta_{wp} \tag{9}$$

The values of these soil hydraulic parameters and properties are visualised in the figures below (**Figure S1**-**Figure S2**).

For the default model version, the percolation parameter $p_b$ is calculated from $b$ as:

$$p_b = 5.87 - 0.29 * b \tag{10}$$

and the parameter $p_e$ is set to 2.

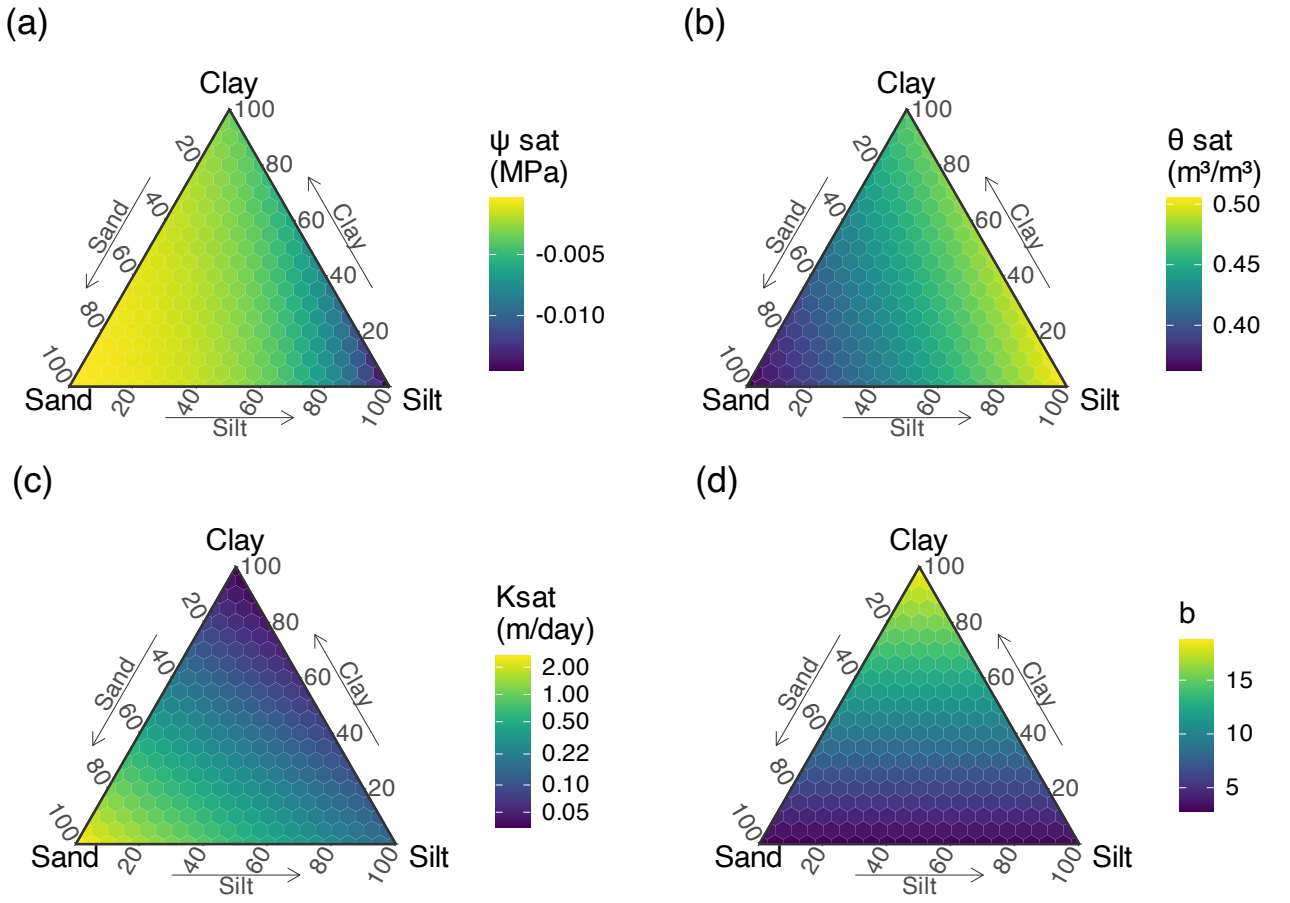


**Figure S1.** Soil hydraulic shape parameters in function of soil texture, based on the pedotransfer functions used in the LPJ-GUESS model (Campbell, 1974). Parameters include (a) soil matric potential at saturation, (b) soil water content at saturation, (c) hydraulic conductivity at saturation (log10 scaled legend colours), and (d) the b shape parameter.

55

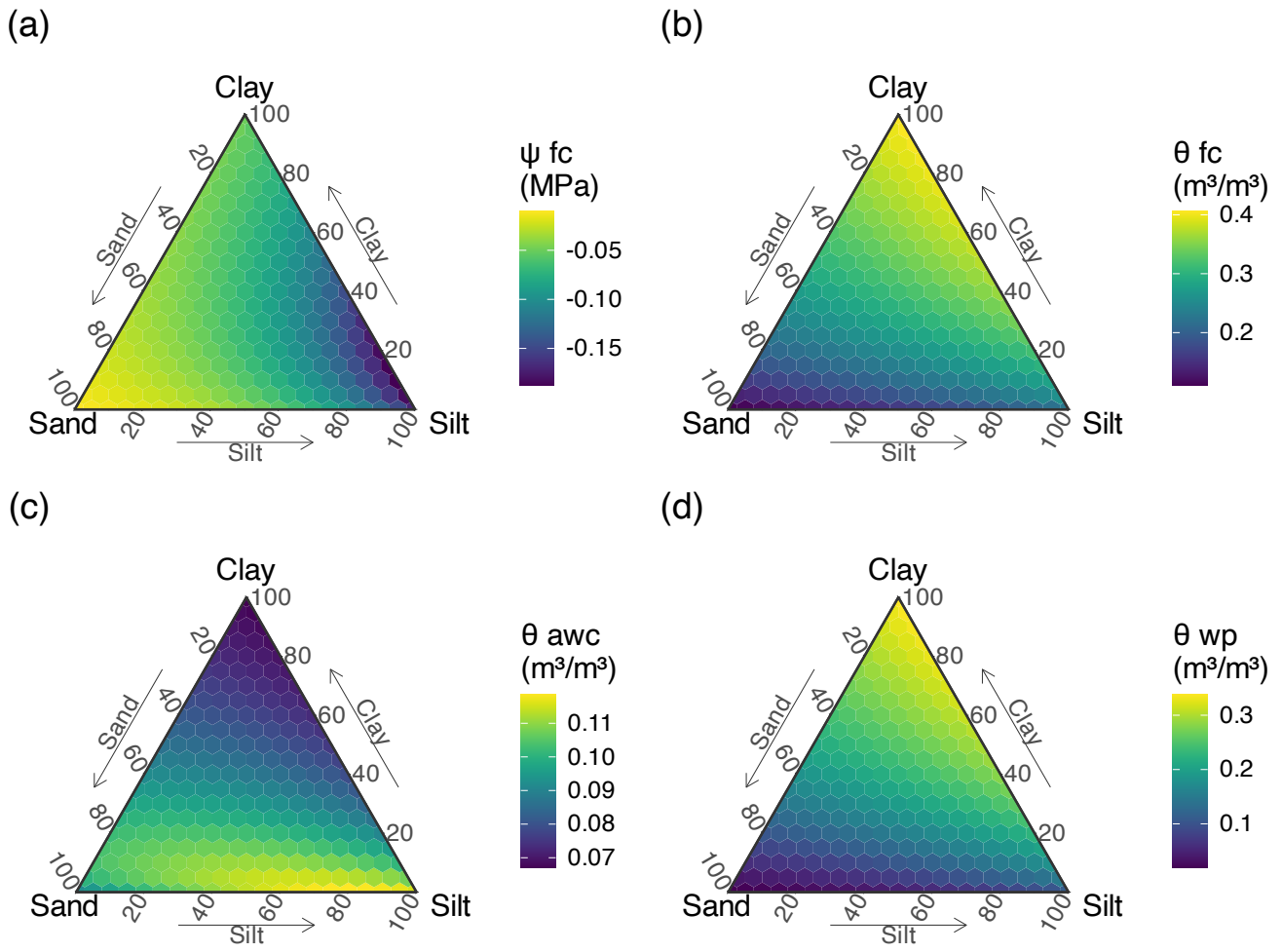


**Figure S2.** Soil hydraulic properties in function of soil texture. Calculated by the pedotransfer functions used in the LPJ-GUESS model. Properties include (a) soil matric potential at field capacity, (b) soil water content at field capacity, (c) plant-available soil water capacity and (d) soil water content at wilting point.

**S1.2 Plant transpiration**

Plant transpiration (Et; mm day$^{-1}$) of a given cohort under well watered conditions (no drought stress) is calculated by the daily atmospheric water demand multiplied by foliar projective cover (FPC) of the cohort:

$$\mathrm{Et} = \mathrm{E}_{\mathrm{demand}} * \mathrm{FPC} \quad (11)$$

Atmospheric demand is calculated from the equilibrium evapotranspiration rate and an empirical relation between evaporation efficiency and surface conductance (Haxeltine and Prentice, 1996; Monteith, 1995; Sitch et al., 2003).

Under drought stress conditions, plant transpiration is reduced to the daily soil water supply ($W_{supply}$) instead:

$$\mathrm{Et} = \mathrm{W}_{\mathrm{supply}} * \mathrm{FPC} \quad (12)$$

Daily plant water supply depends on the soil water availability and is further limited by a parameter *emax*, which represents the daily maximum transpiration (mm day$^{-1}$) rate for a given PFT:

$$\mathrm{W}_{\mathrm{supply}} = \mathrm{emax} * \mathrm{wr} \quad (13)$$

where *wr* represents the water uptake as a fraction of the maximum possible, given as the sum over the fractions (*fwuptake*) for each soil layer. The default version of LPJ-GUESS v4.1 has four different ways to parameterise the fraction of plant water uptake from each soil layer (Nord et al., 2021). For the default benchmark simulations, as well as all simulations used in this manuscript, the "rootdist" scheme is used. In this parameterisation, plant water uptake is modelled as being independent of soil water content (down to wilting point, below which it will be zero) but having a fractional uptake from the different soil layers according to the prescribed root distribution (*rootdist*). For a given soil layer *s*, this fraction is given by:

$$fwuptake(s) = min\big(wcont(s) * awc(s) * fpc_r, emax * rootdist(s)\big)/emax \quad (14)$$

Where *wcont* is the fractional water content between wilting point and field capacity, *awc* is the plant-available water holding capacity, and $fpc_r$ is a rescaling factor to account for foliar overlap between cohorts.

### S1.3 Surface evaporation

Soil surface evaporation (Es) is initially calculated based on the daily equilibrium evaporation (EET):

$$Es = EET * PT * fevap * wcont^2 \quad (15)$$

where EET is the equilibrium evaporation, PT = 1.32 is the Priestley-Taylor coefficient, which converts equilibrium evaporation into potential evaporation ($E_{pot}$ = $EET * PT$), *fevap* is the bare soil fraction of the patch, and *wcont* is the water content (fraction between $\theta_{wp}$ *and* $\theta_{fc}$) in the evaporation layer (Rost et al., 2008). Here EET is calculated from temperature and radiation flux, see Equation 5 in Prentice et al. (1993). In the next step, this initial Es value may be further reduced. If plant transpiration reduces $\theta$ in the top soil layer such that not enough water is available to meet Es, the value of Es will be reduced to match water content that is still available.

### S1.4 Interception loss

Evaporation from canopy interception is calculated as in (Gerten et al., 2004). For the cohort vegetation representation in LPJ-GUESS (Nord et al., 2021) the daily interception loss (mm/day) by each cohort is calculated as

$$Ei = fwet * E_{pot} * FPC \quad (16)$$

where *fwet* is the fraction of the day that the canopy remains wet. It is calculated as the minimum of $fpc_r$ (a rescaling factor to account for canopy overlap between cohorts, $fpc_r = 1/\max(FPC_{tot},1)$) and $S_I/E_{pot}$ where $S_I$ is the storage capacity (mm/day) for precipitation by the canopy, calculated as

$$P * min(LAI * intc, 1) \quad (17)$$

where P is daily precipitation (mm/day) and *intc* is the interception coefficient, a dimensionless PFT parameter that represents the rainfall regimes effect, with default values of 0.01 for grasses, 0.02 for broadleaf trees, and 0.06 for needleleaf trees. (Gerten et al., 2004; Kergoat, 1998; Nord et al., 2021). Cohort-level interception losses are finally added up to the patch level.

## S2 Implementation of Richard's equations in LPJ-GUESS

The following code snippets form the heart of our new hydrology module in our version of the LPJ-GUESS model. These snippets are inserted in the **soil.cpp** file of the LPJ-GUESS code and can be found as part of the "hydrology_openRE()" function. More small changes in the code are needed for the update to function, and for this we refer to the full code (Verbruggen et al., 2025).

Here we first initiate a system of differential equations (called "openREsys" after Ireson et al. (2023)) and integrate it over one day. The differential equation solver with adaptive timestep will automatically determine the necessary subdaily timesteps needed to minimize mass balance errors.

```
// Define ODE system
openREsys re(transp_layer,evap,water_infilt,patch.soil);

// Preparation for the ODE integrator
typedef std::vector< double > state_type;
typedef boost::numeric::odeint::runge_kutta_cash_karp54< state_type > stepper_type;

// This line will perform the integration
size_t integrationSteps = boost::numeric::odeint::integrate_adaptive(
                                    boost::numeric::odeint::make_controlled< stepper_type >( 1.0e-4 , 1.0e-6 ),
                                    re,F,0.0,1.0,0.025
                          );
```

The following code snippet defines the system of differential equations (Richards equation) that is used to update soil water content every subdaily timestep, including the different bottom boundary conditions.

```
class openREsys {

            private:

                        // Shortcuts
                        const int N = NSOILLAYER;
                        const double m2MPa = 0.00978057; // [MPa] convert meter of head to MPa (same sign)

                        double (&Transp)[NSOILLAYER]; // transpiration from each soil layer [mm/day]
                        double& evap;
                        double& waterinfilt;
                        Soil& soil;

            public:

                        // Set up the constructor.
                        openREsys(double (&tr)[NSOILLAYER], double& evapobj, double& waterinfiltobj, Soil& soilobj) :
                                    Transp(tr),
                                    soil(soilobj),
                                    evap(evapobj),
                                    waterinfilt(waterinfiltobj) {}

                        // And this is the actual dFdt calculator function.
                        void operator()(std::vector<double> &x, std::vector<double> &dxdt, double t){

                                    //
                                    // PREPARATION
                                    //

                                    // Temporary stuff
                                    double reP[N], reK[N], reC[N]; // layer psi (P), hyd. conductivity (K) and specific moisture capacity
(C)
                                    double reQ[N+1];      // layer edge water fluxes
                                    double lyrdist = 0.0; // distance between centers of neigbouring layers lyrdist = (dz(i)+dz(i+1))/2
```

```
                        // Note that F = x in this class. Sorry.
                        // F[0]   = upper boundary condition
                        // F[N+1] = lower boundary condition
                        // F[1:N] = psi [m]

                        // Calculate P's, K's and C's for this calculation timestep
                        for(int i = 0; i<N; i++){
                                    x[i+1] = max(-1e8,min(0.0,x[i+1])); // Force x to stay within bounds
                                    reP[i] = x[i+1]; // [m]
                                    reK[i] = (24*60*60)*soil.calc_K(reP[i]*m2MPa); // [m/day]
                                    reC[i] = soil.calc_C(reP[i]*m2MPa); // [1/m]
                        }

                        //
                        // RICHARDS EQUATION
                        //

                        // Top layer boundary condition: water input minus evaporation
                        reQ[0] = (waterinfilt - evap)/1000; // [m/day]

                        // Bottom boundary condition
                        double psibottom = 0;
                        double kbottom = 0;
                        switch(soil_bottombound){
                        case AQUIFER:
                         {
                          psibottom = soil.soiltype.psi_sat; // [m] fixed psi boundary (Eq. 14 in Ireson et al. 2023)
                          kbottom = (24*60*60)*soil.soiltype.Ksat; // [m/day]
                          reQ[N] = -((reK[N-1]+kbottom)/2)*((psibottom-reP[N-1])/(soil.soiltype.Dz_layer[N-1]/(2*1000))-1);
                          break;
                        }
                        case FREEDRAINAGE:
                         {
                          reQ[N] = reK[N-1]; // free drainage (Eq. 13 in Ireson et al. 2023)
                          break;
                        }
                        case BEDROCK:
                         {
                          reQ[N] = 0; // zero flow through lower edge of bottom layer
                          break;
                         }
                        }

                        // Calculate fluxes at the edges of the soil layers (q)
                        for(int i=1; i<N; i++){
                          lyrdist = (soil.soiltype.Dz_layer[i-1]+soil.soiltype.Dz_layer[i])/2;
                          reQ[i] = -((reK[i]+reK[i-1])/2)*((reP[i]-reP[i-1])/(lyrdist/1000)-1);
                        }

                        // Finally we can calculate dFdt. This corresponds to Eq. 10 in Ireson et al. 2023
                        // - The added Transp represents water loss from plant transpiration [mm/day] for this layer.
                        // - reQ[0] and reQ[N] will be integrated over the calculation timestep,
                        //   so they will give the cumulative fluxes.

                        // Note that we have to be very careful with the indices here...!
                        // Some hints:
                        // - reC and Transp have length N (so indices should not reach N because we start from zero)
                        // - reQ has length N+1
                        // - dxdt has length N+2

                        dxdt[0]   = reQ[0];
                        dxdt[N+1] = reQ[N];
                        for(int i = 1; i <= N; i++){
                         dxdt[i] = -(1/reC[i-1])*(reQ[i]-reQ[i-1]+(Transp[i-1]/1000))/(soil.soiltype.Dz_layer[i-1]/1000);
                        }

                    }
};
```

## S3 Model setup

### S3.1 Plant functional types

**Table S1.** Plant functional types that were activated in the LPJ-GUESS models used in this paper. Parameter values used from Verbruggen et al. (2024). Parameters include specific leaf area (SLA), daily maximum transpiration rate ($e_{max}$), tree leaf to sapwood cross-sectional area ratio ($k_{latosa}$), allometric parameters to convert between height and diameter at breast height ($k_{allom1}$, $k_{allom2}$), maximum crown area ($crownarea_{max}$), root distribution shape parameter ($\beta_{root}$), and wood density.

| PFT | Parameter (units) | Value |
|---|---|---|
| $C_4$ Grass | SLA ($m^2$/kgC) | 35.31 |
| | $e_{max}$ (mm/d) | 7 |
| Tropical Shrubs | SLA ($m^2$/kgC) | 25.63 |
| | Wood density (kgC/$m^3$) | 361.57 |
| | $e_{max}$ (mm/d) | 7 |
| | $k_{latosa}$ | 4000 |
| | $k_{allom1}$ | 250 |
| | $k_{allom2}$ | 8 |
| | $crownarea_{max}$ ($m^2$) | 5 |
| | $\beta_{root}$ | 0.9659 |
| Tropical Evergreen Trees | SLA ($m^2$/kgC) | 13.89 |
| | Wood density (kgC/$m^3$) | 319.06 |
| Tropical Raingreen Trees | SLA ($m^2$/kgC) | 25.70 |
| | Wood density (kgC/$m^3$) | 318.725 |

### S3.2 Gap-filling of meteorological drivers

Daily meteorological drivers from the fluxtower site in Dahra Senegal for 2002–2022 were gap-filled using the following procedure. First, subdaily (15 minute) data of air temperature at 2m, short-wave incoming radiation, relative humidity (2m), wind speed (2m) and precipitation were collected. Gaps of 6 time-steps (2 hours) or less were filled by interpolation. Subdaily drivers were then aggregated to daily average rates, leaving empty any incomplete days. Next, any gaps of 2 days or less in the daily aggregates were filled by interpolation. Missing rainfall data during the dry season (October–May) were assumed to be zero. Missing rainfall data during the wet season were gap-filled by using rainfall from the Multi-Source Weighted-Ensemble Precipitation, version 2 (MSWEP V2) data product (Beck et al., 2019). Yearly totals of the MSWEP data product were scaled to match yearly Dahra fluxtower rainfall data, after removing from both datasets any days for which the Dahra data were missing. This yearly scaling factor was then used to scale the daily MSWEP data for the given year, which were

then used to fill in any remaining gaps in the fluxtower data. In other words, instead of simply inserting the pure MSWEP data, we take into account the performance of MSWEP for the non-missing data in each given year. Data for the other meteorological drivers were taken from the ERA5-Land data product (Muñoz-Sabater et al., 2021) and scaled similarly.

**S3.3 Soil texture input maps**

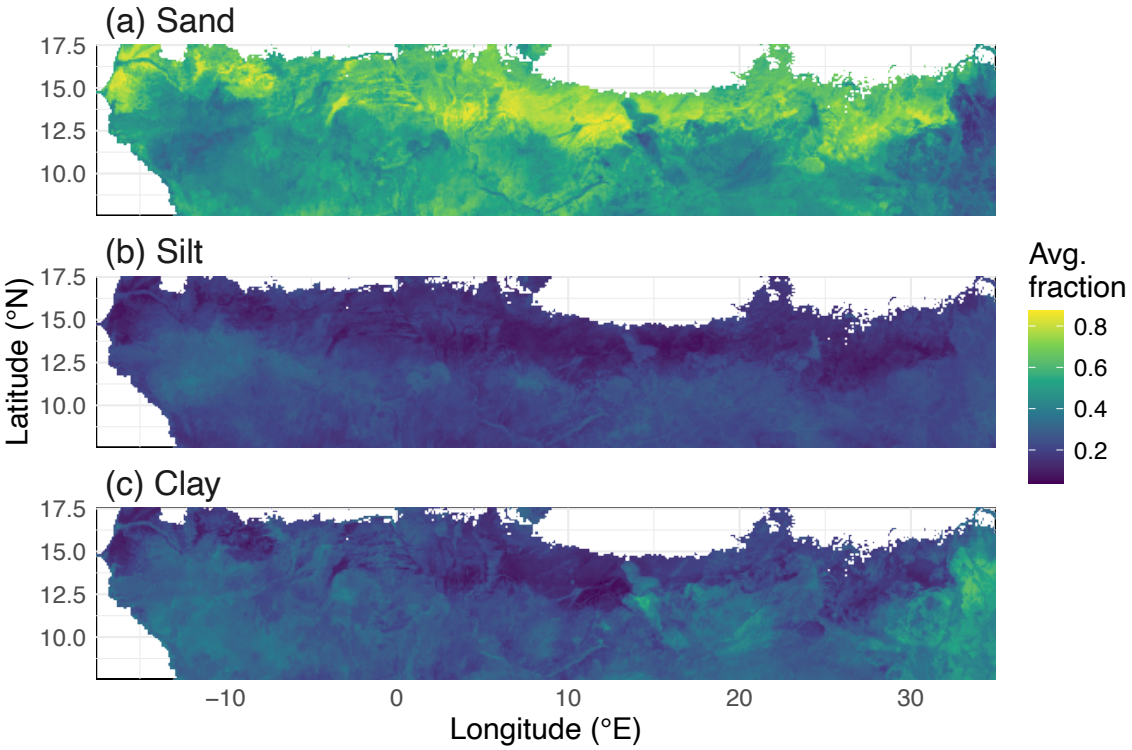


**Figure S3.** Soil texture (sand, silt and clay fractions) from the ISRIC Africa SoilGrids, regridded to 0.1° resolution and averaged over the different soil depths in the database (Hengl et al., 2015).

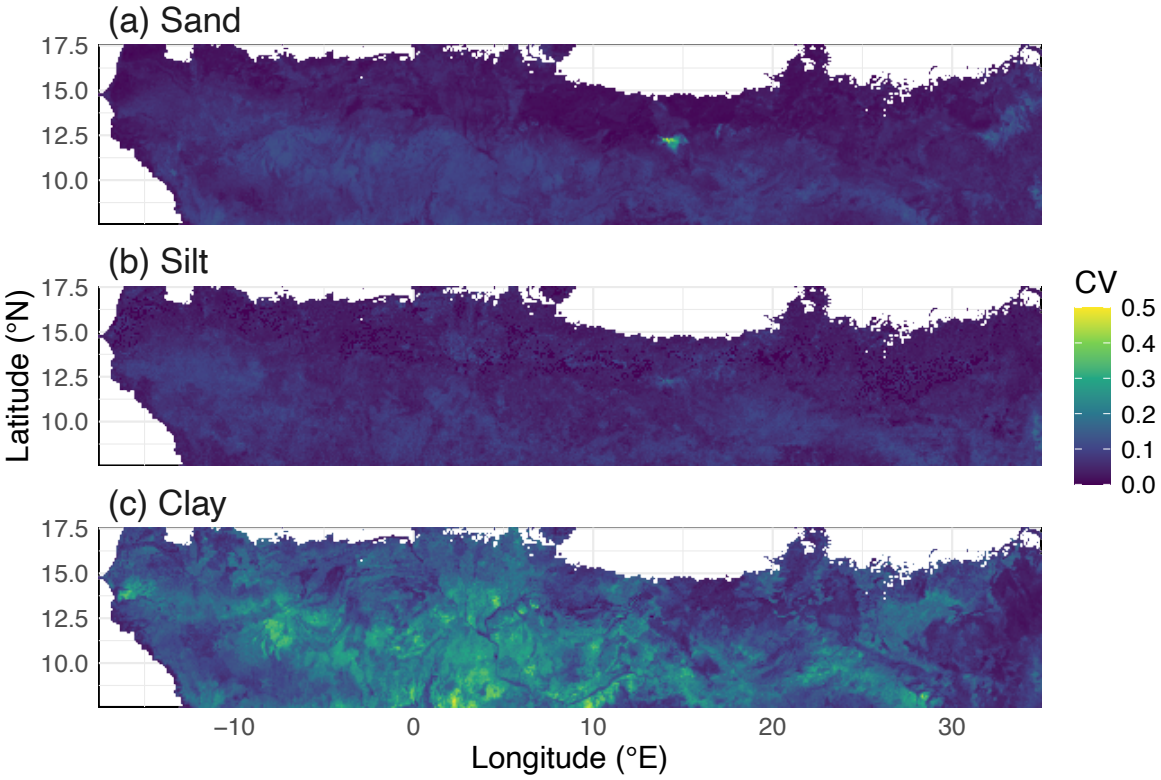


**Figure S4.** Variation in soil texture between the six layers in the Africa SoilGrids database (Hengl et al., 2015). Variation is shown as a coefficient of variation (CV = st.dev / avg) over all layers.

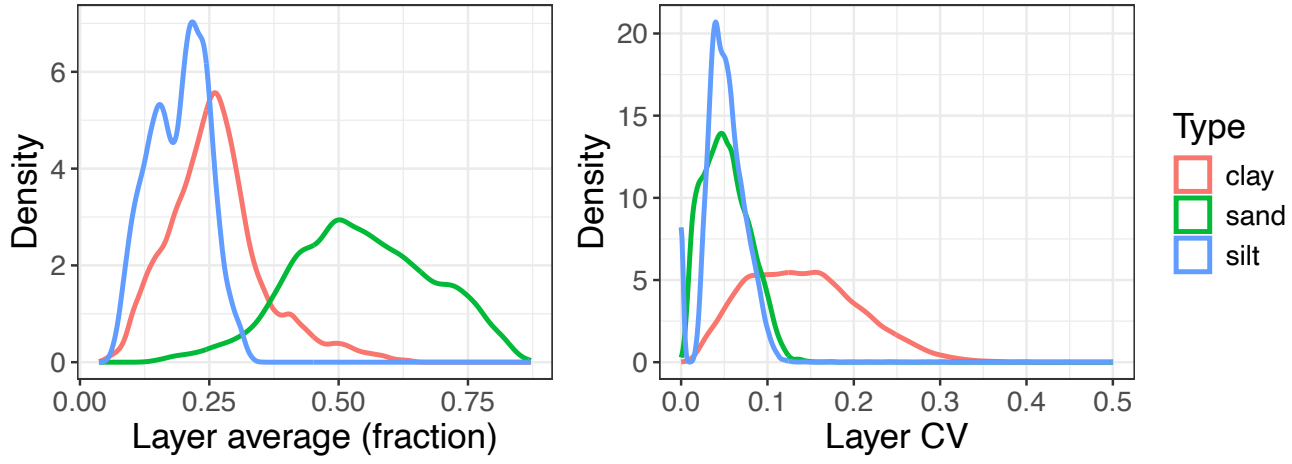


**Figure S5.** Distribution of inter-layer average (left) and CV (right) for all simulated gridcells in the Sahel, derived from the Africa SoilGrids database (Hengl et al., 2015).

## S4 Additional results

### S4.1 Model performance at Dahra fluxtower site

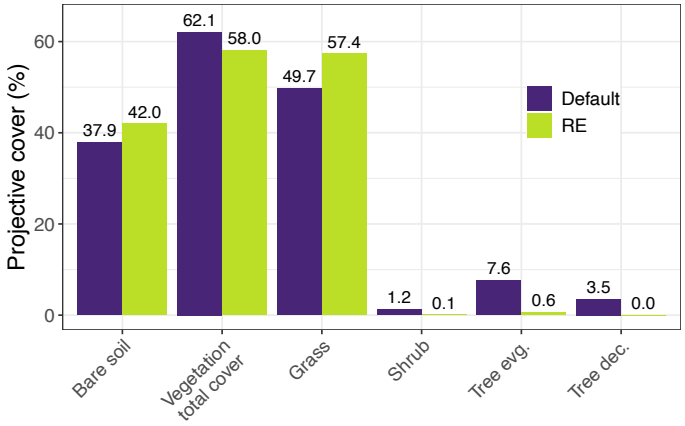


**Figure S6.** Simulated average projective cover of the different vegetation types, the total vegetation cover, and the bare soil fraction (complement of the total vegetation cover) for the Dahra fluxtower site in Senegal. Average taken over the years 2002–2022 for the default LPJ-GUESS v4.1 model version (Default) and the updated version (RE).

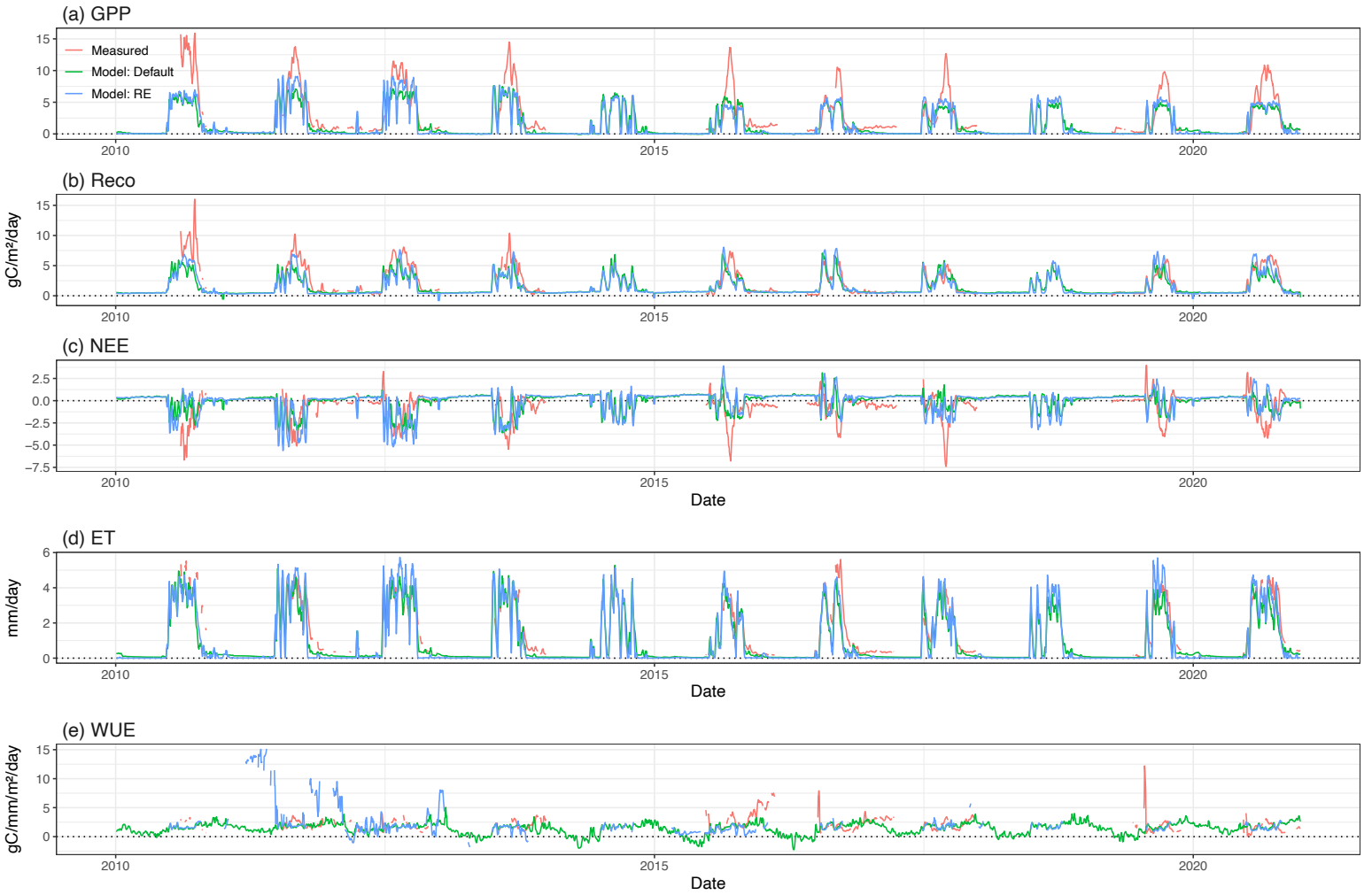


**Figure S7.** Full time series of measured vs. simulated (*a–c*) carbon fluxes, *(d)* water fluxes and (*e*) water use efficiency at the Dahra site in Senegal for the period 2010–2020. Both the standard ("Default") and the updated ("RE") model versions of LPJ-GUESS v4.1 are compared against measurements of *(a)* GPP, *(b)* Reco, *(c)* NEE and *(d)* ET, as well as the derived WUE (*e*). Figures show 5-day moving averages for all variables.

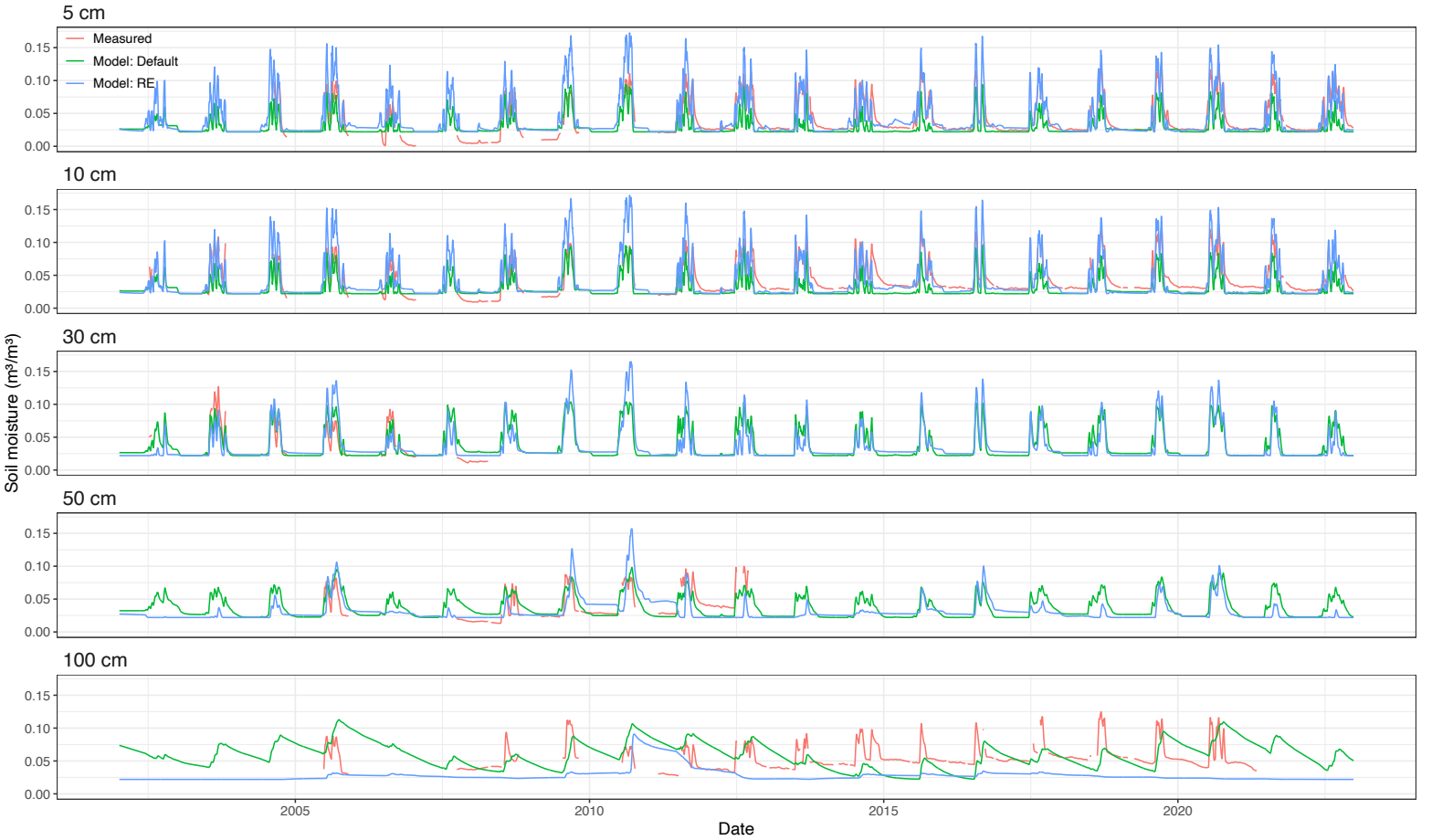


**Figure S8.** Time series measured vs. simulated volumetric soil moisture content at the Dahra site in Senegal for 2002–2022. Panels show 5-day moving averages of results at different soil layer depths (5–100cm). Simulated results were interpolated to match observed layer depths.

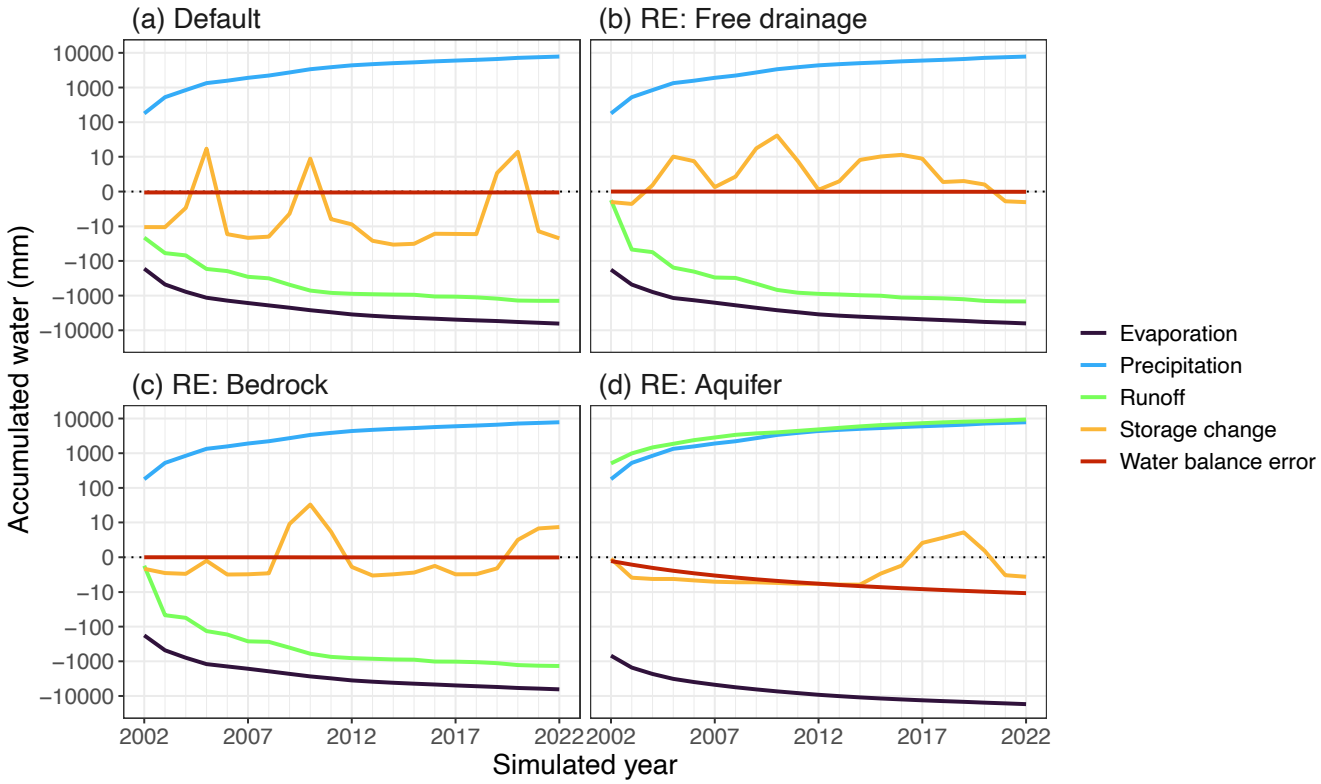


**Figure S9.** Hydrological components of the water mass balance for the different model versions, shown as cumulative sums over 2002–2022 for the Dahra fluxtower site. The different hydrological components correspond to the terms in Eq. 13 of the main text.

## S4.2 Regional performance

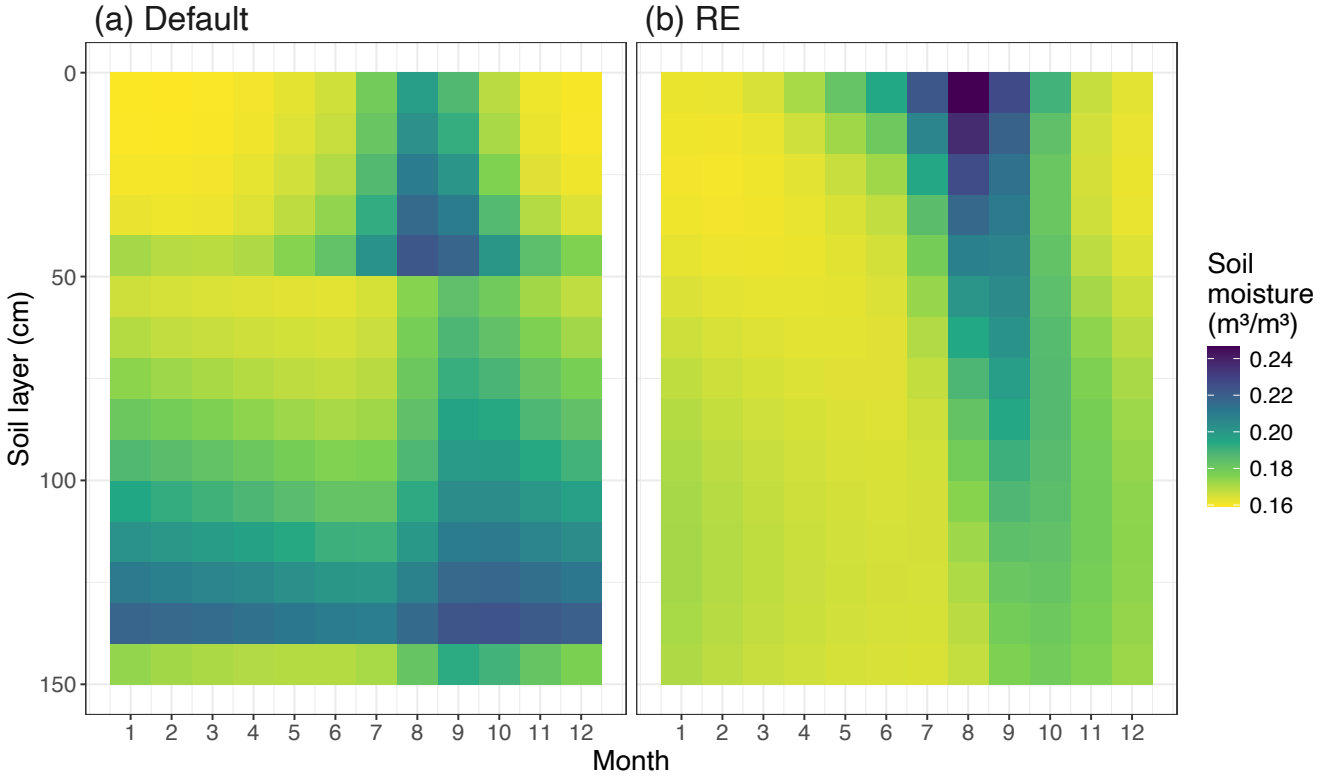


**Figure S10.** Average yearly cycle of simulated monthly soil moisture ($m^3/m^3$) for the Sahel region, averaged over all grid cells. Panels show the simulations by (a) the default version of LPJ-GUESS v4.1 and (b) the updated version based on Richards equation with a free drainage bottom boundary condition.

## S4.3 Impacts on simulated regional vegetation cover

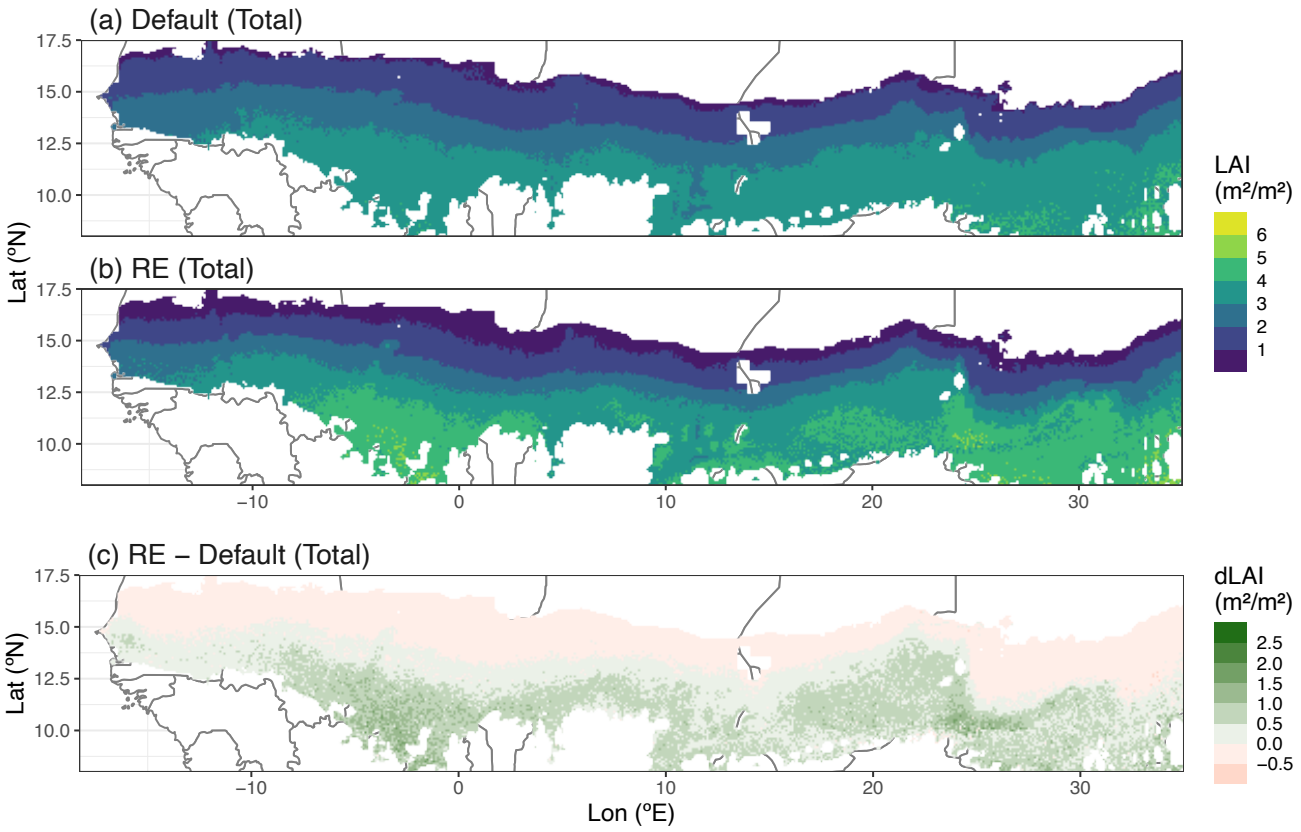


**Figure S11.** Regional model output of vegetation leaf area index (LAI) for vegetation total. Yearly maximum LAI was averaged over the period 1980–2022 for (a) the default version of LPJ-GUESS and (b) our RE-based version. Models are compared in panel (c) by taking the difference of both model's outputs.

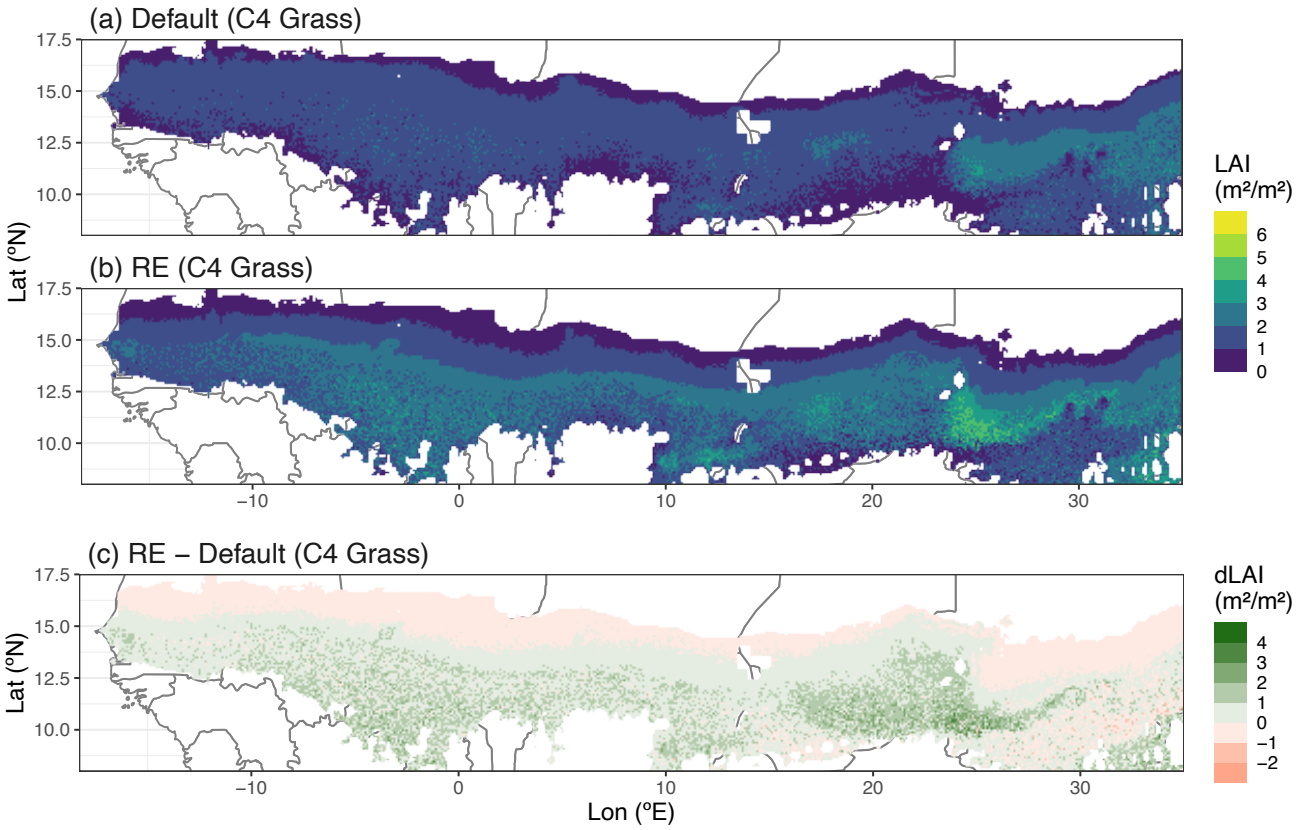


310

**Figure S12.** Regional model output of vegetation leaf area index (LAI) for the $C_4$ grass PFT. Yearly maximum LAI was averaged over the period 1980–2022 for (a) the default version of LPJ-GUESS and (b) our RE-based version. Models are compared in panel (c) by taking the difference of both model's outputs.

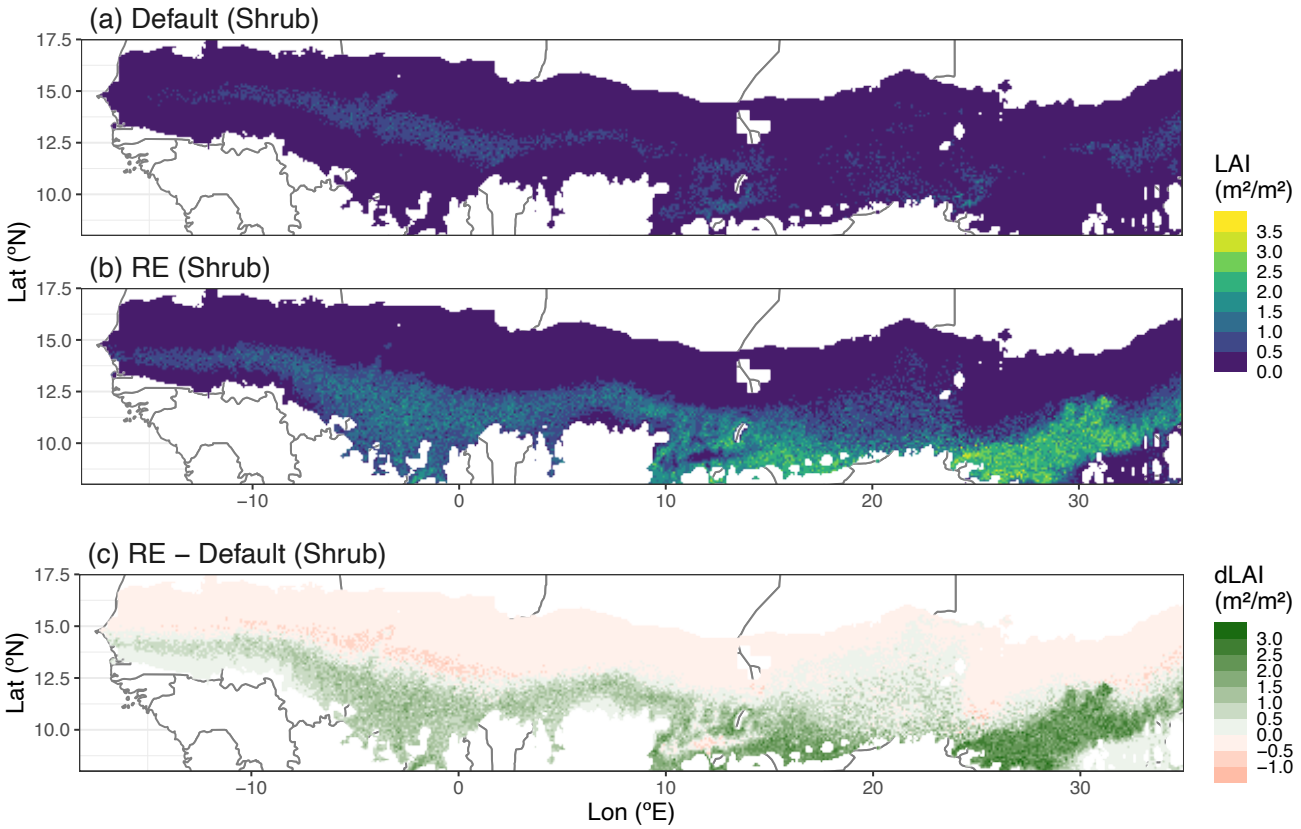


315 **Figure S13.** Regional model output of vegetation leaf area index (LAI) for the tropical shrub PFT. Yearly maximum LAI was averaged over the period 1980–2022 for (a) the default version of LPJ-GUESS and (b) our RE-based version. Models are compared in panel (c) by taking the difference of both model's outputs.

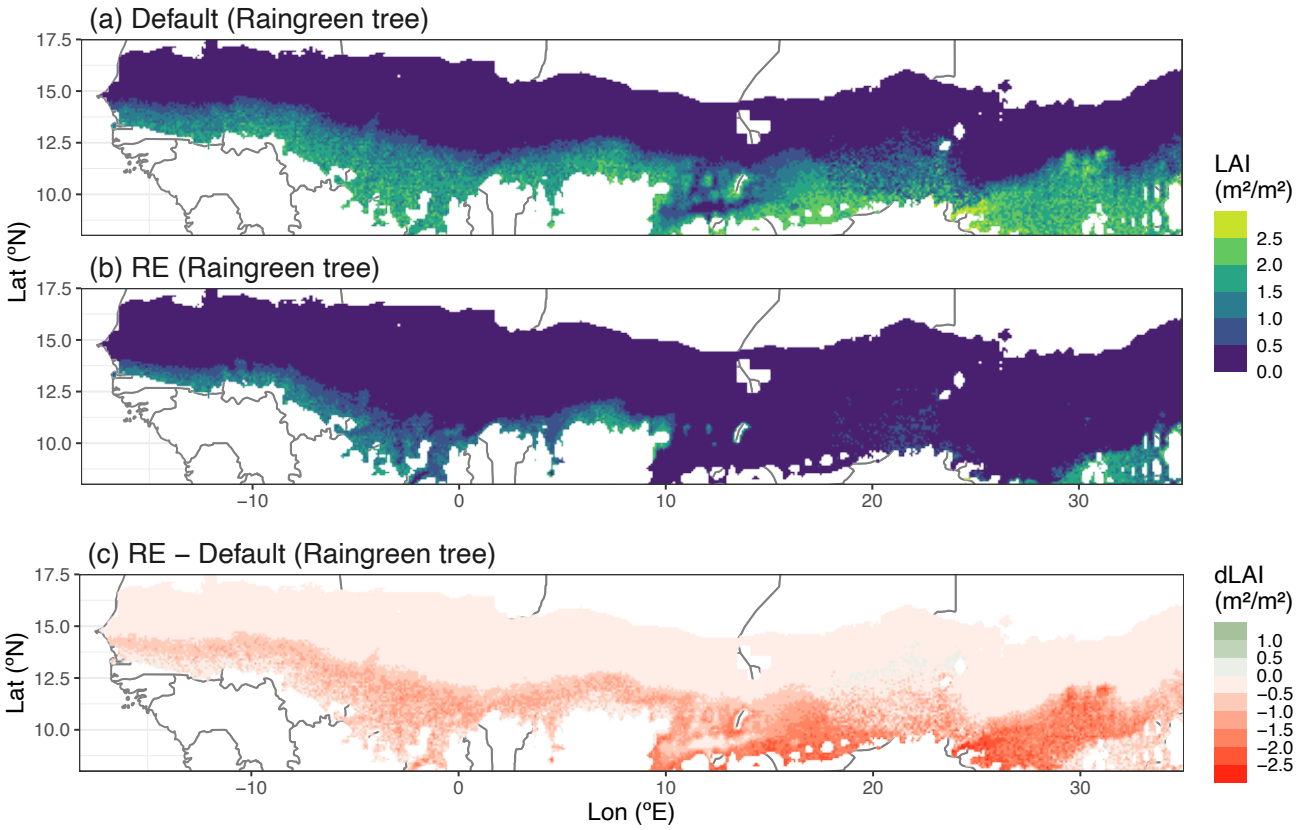


320 **Figure S14.** Regional model output of vegetation leaf area index (LAI) for the raingreen tree PFT. Yearly maximum LAI was averaged over the period 1980–2022 for (a) the default version of LPJ-GUESS and (b) our RE-based version. Models are compared in panel (c) by taking the difference of both model's outputs.

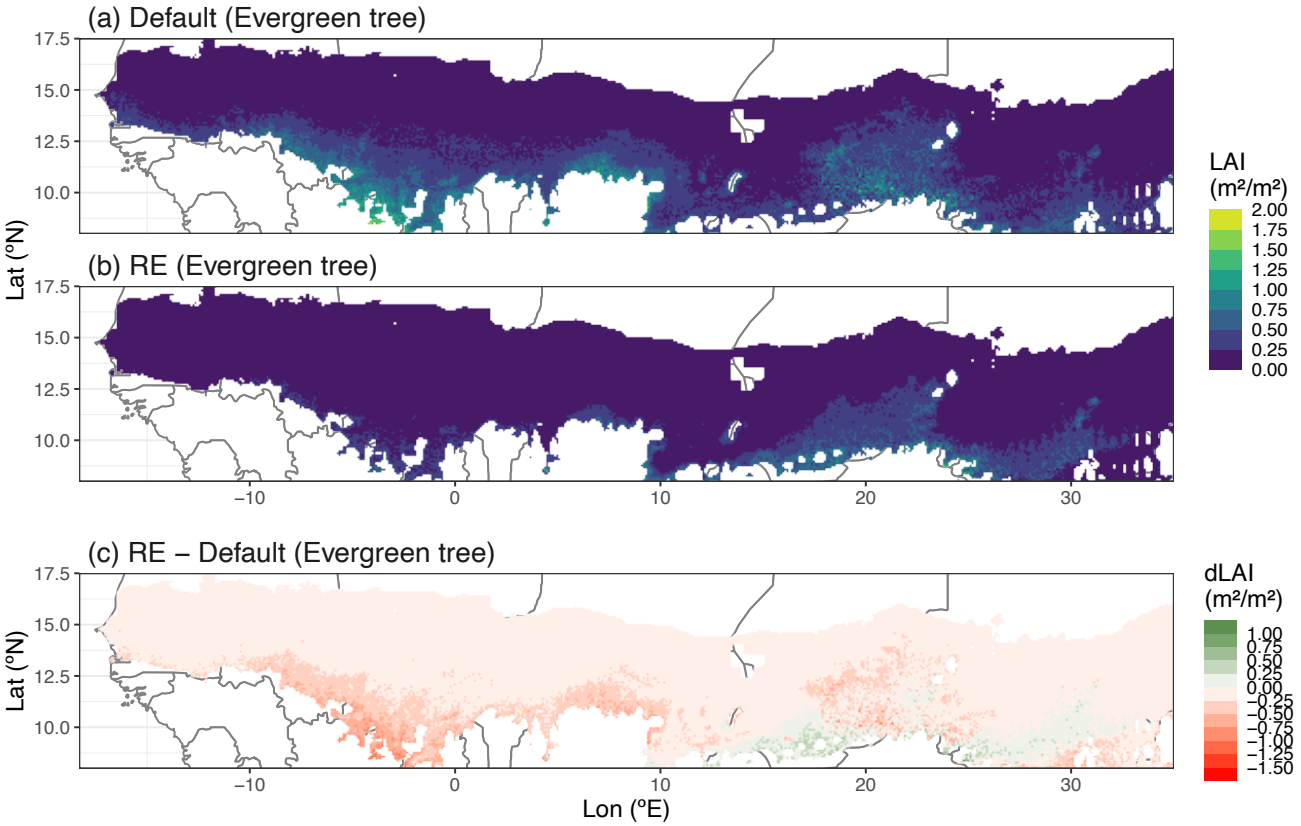


325 **Figure S15.** Regional model output of vegetation leaf area index (LAI) for the evergreen tree PFT. Yearly maximum LAI was averaged over the period 1980–2022 for (a) the default version of LPJ-GUESS and (b) our RE-based version. Models are compared in panel (c) by taking the difference of both model's outputs.

## S4.4 Soil texture sensitivity

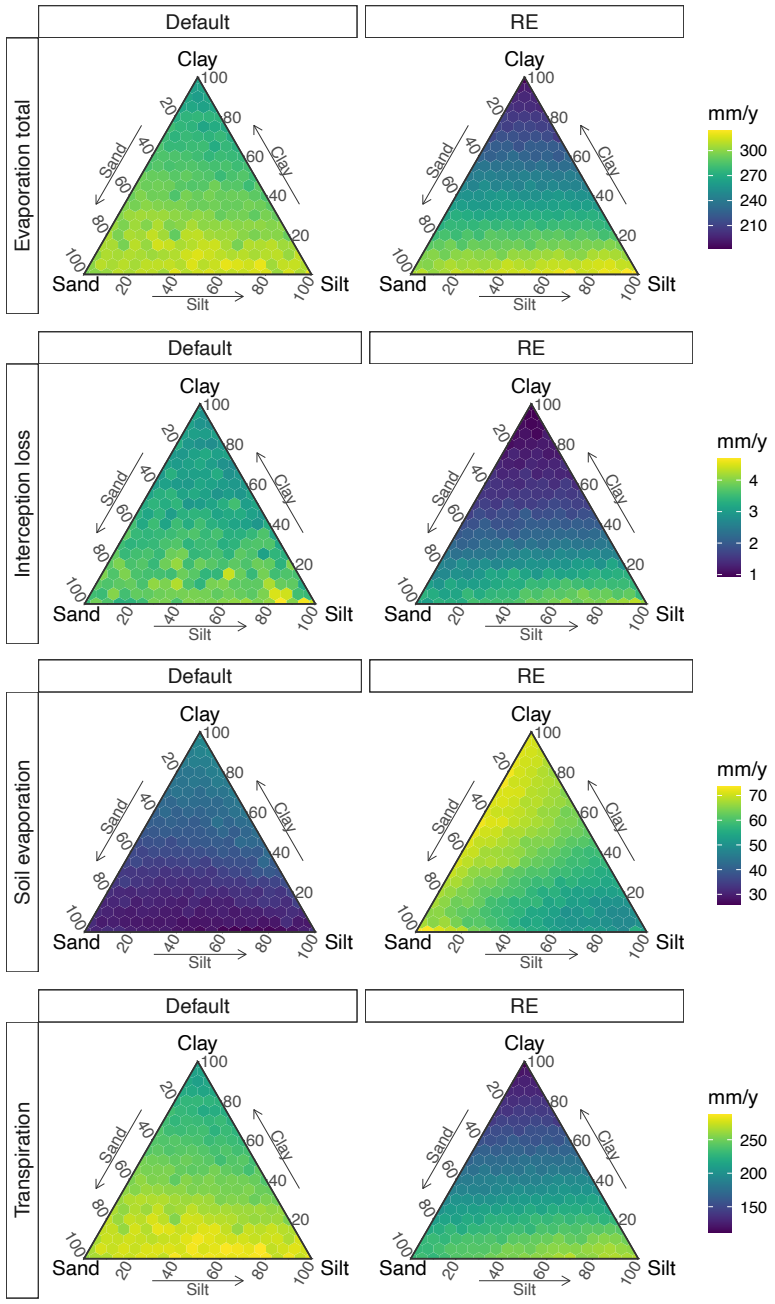


**Figure S16.** Simulated sensitivity of evaporation components (rows) to soil texture for both model versions (columns), based on the Dahra meteorological drivers. Sensitivities represented by ternary plots of time-series average evaporation component values for each soil type.

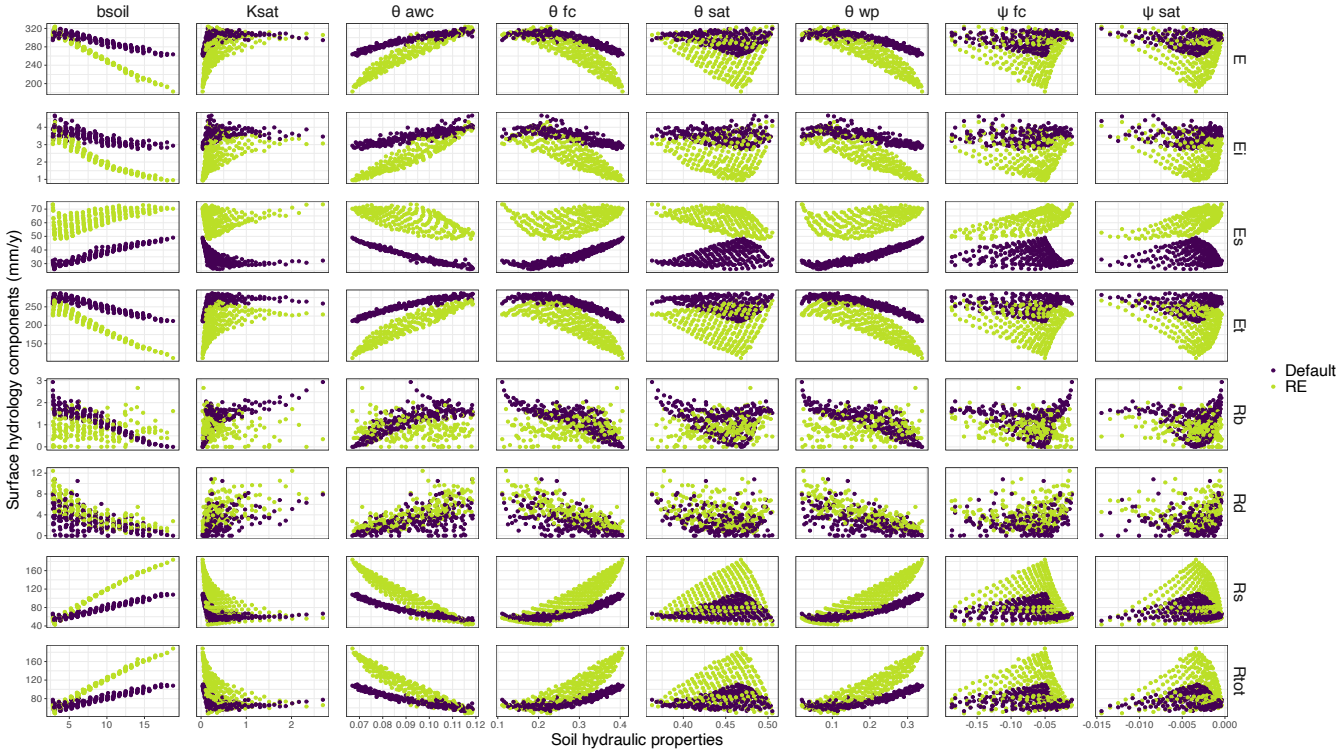


**Figure S17.** Results of sensitivity test of soil texture on simulated surface hydrology presented in function of derived soil hydraulic properties for each soil texture. Colours represent different model versions (default vs. RE-based). Units for $\psi$ are MPa, units for $\theta$ are $m^3/m^3$, and units for $K_{sat}$ are m/day. Surface hydrology components include total evaporation (E), evaporation by interception loss ($E_i$), bare-soil evaporation ($E_s$), plant transpiration ($E_t$), baseflow runoff ($R_b$), lateral drainage ($R_d$), surface runoff ($R_s$) and total runoff ($R_{tot}$).

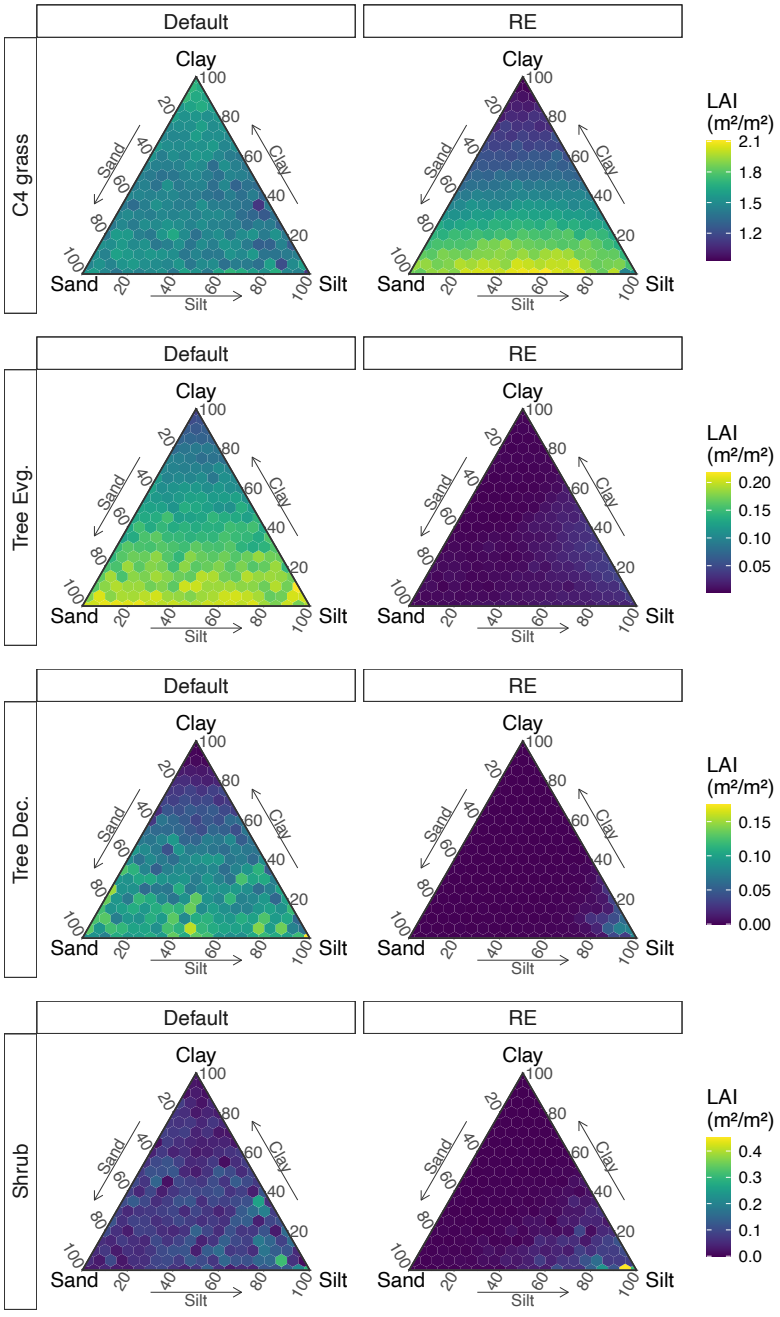


340

**Figure S18.** Simulated sensitivity of the different dryland PFTs (rows) to soil texture for both model versions (columns), based on the Dahra meteorological drivers. Sensitivities represented by ternary plots of time-series average LAI for each soil type.

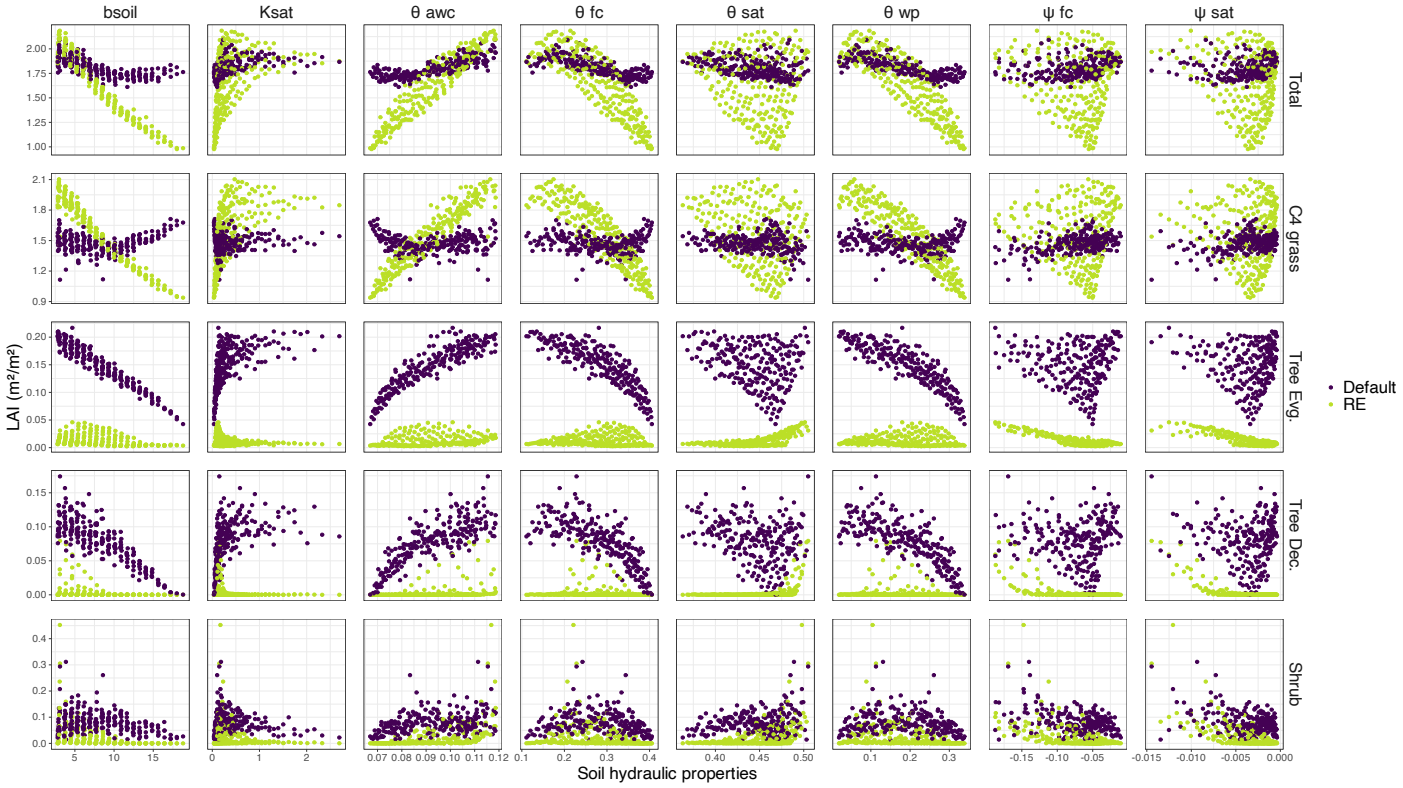


**Figure S19.** Results of sensitivity test of soil texture on simulated vegetation LAI, presented in function of derived soil hydraulic properties for each soil texture. Colours represent different model versions (default vs. RE-based). Units for $\psi$ are MPa, units for $\theta$ are $m^3/m^3$, and units for $K_{sat}$ are m/day.

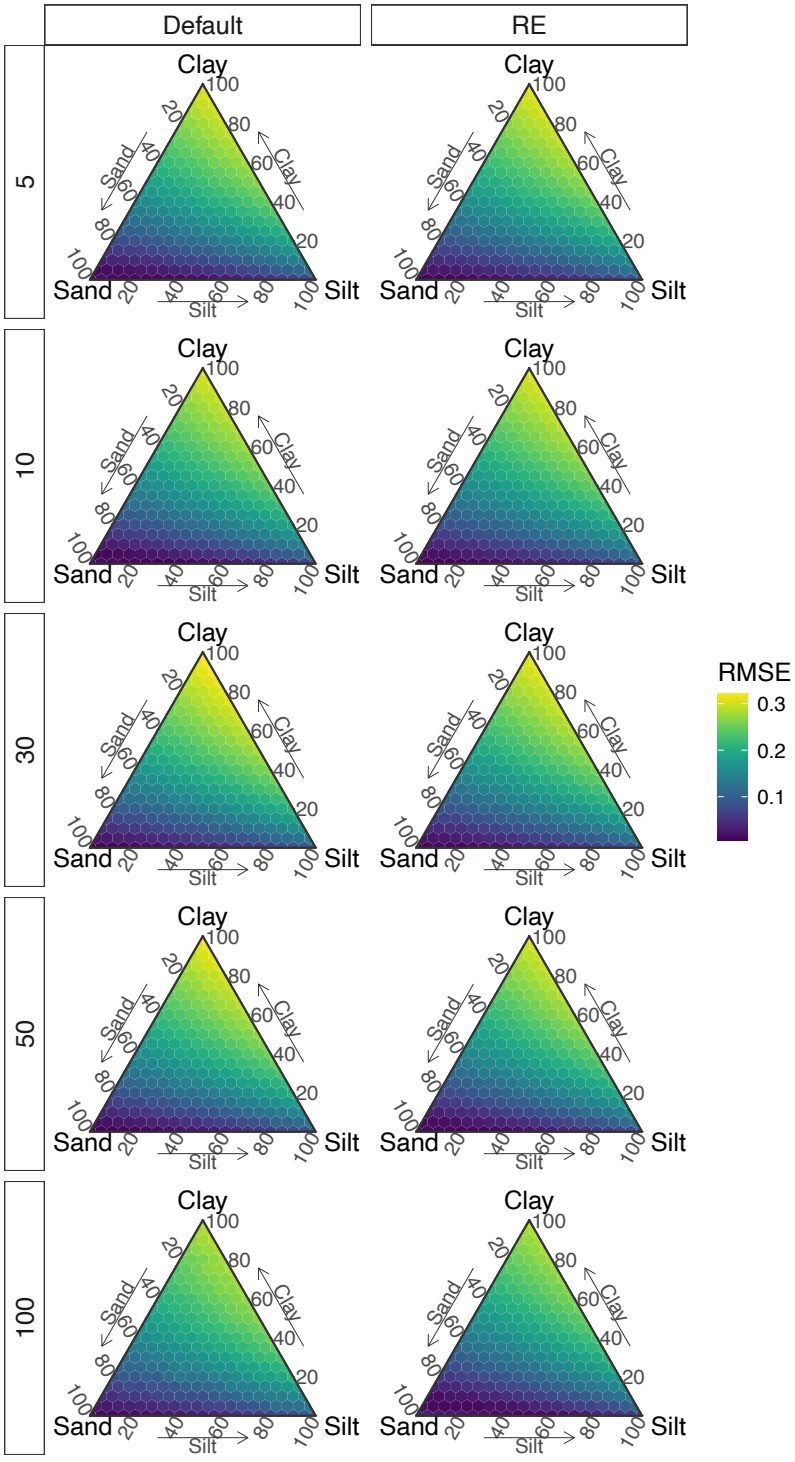


**Figure S20.** Evaluation of simulated soil moisture (average yearly cycle) against measurements from Dahra, Senegal, for both models (columns) in function of soil texture (hexagons) and layer depth (rows).

**S4.5 Groundwater depth**

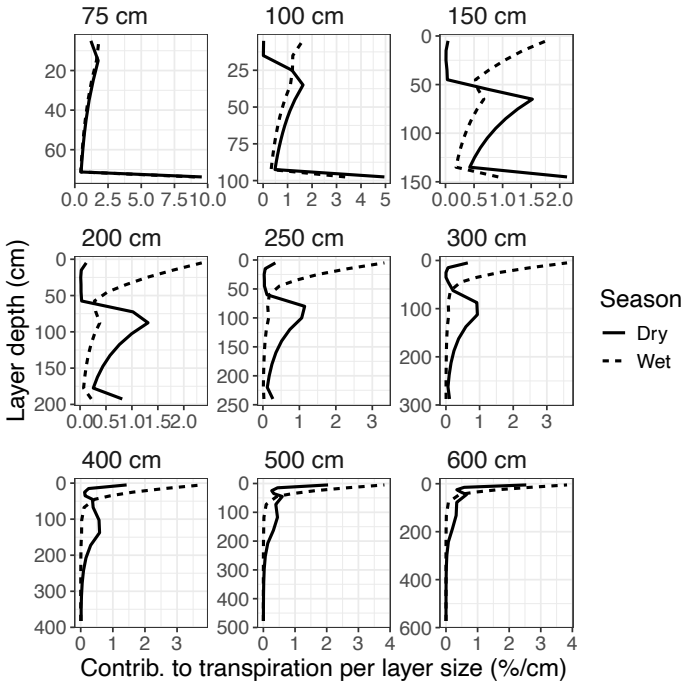


**Figure S21.** Contribution of each soil layer to the simulated total plant transpiration, weighted by soil layer thickness (1/cm), at the Dahra flux tower site, for a selection of ground water depths, ranging from 75–600 cm (panels). Results are averaged over all simulated years (2002–2022) and further separated into the dry and wet season.

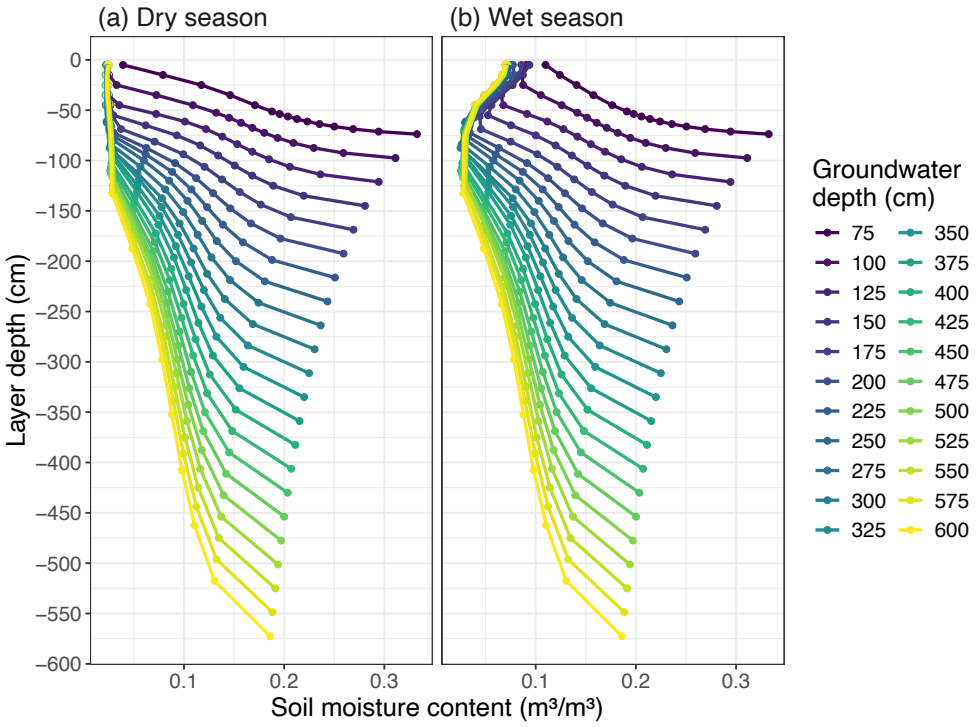


**Figure S22.** Soil moisture content in function of soil layer depth, for different ground water depth values (75–600 cm), at the Dahra flux tower site. Results are averaged over all simulated years (2002–2022) and further separated into the dry and wet season.

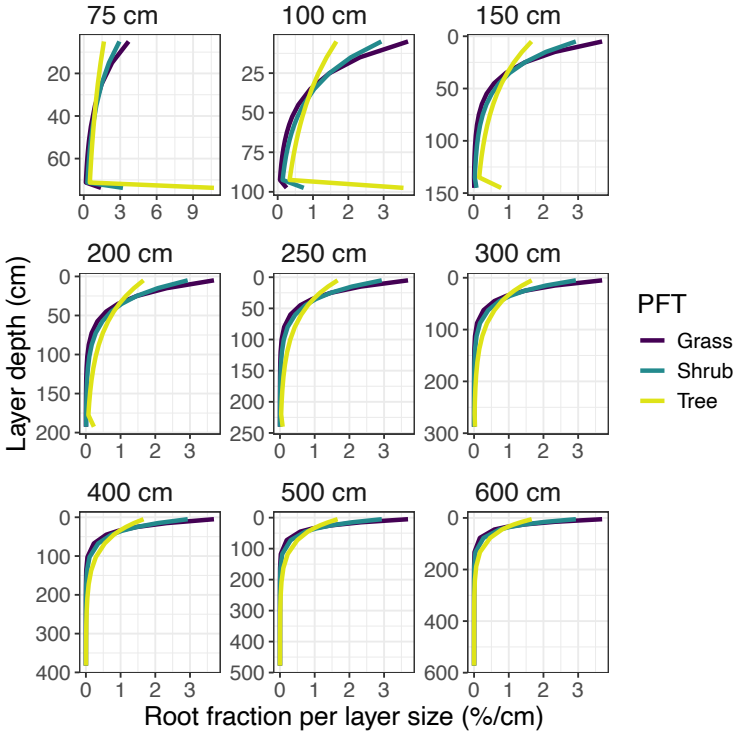


365 **Figure S23.** Root distribution for the different PFT groups, as calculated by the LPJ-GUESS model for a selection of soil depths (75–600 cm; panels). Root distribution weighted by layer size.

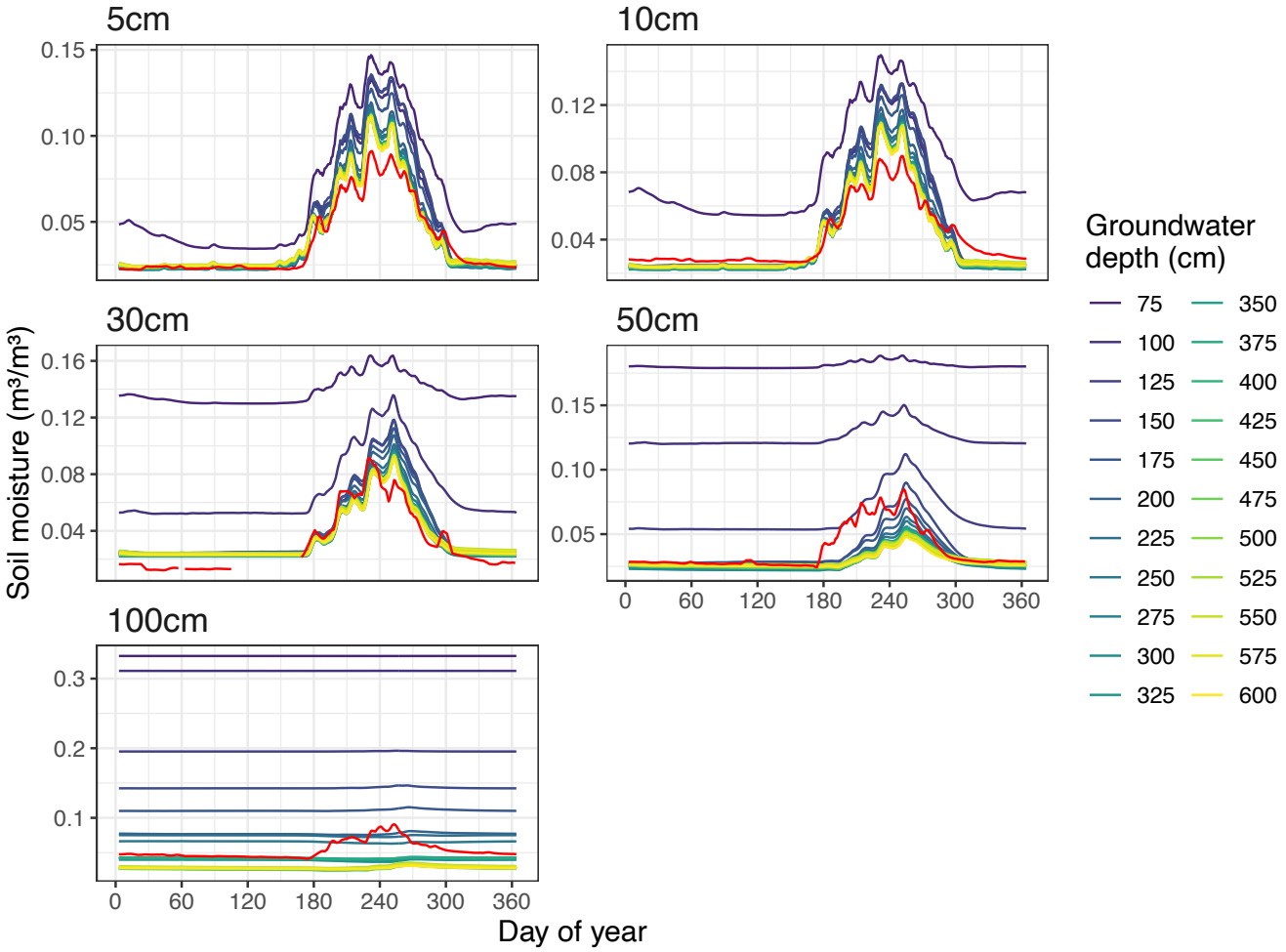


**Figure S24.** Average yearly cycle of measured (red) vs. simulated volumetric soil moisture content at the Dahra site in Senegal for 2002–2022. Model simulations are from the RE-based model, using the "aquifer" bottom boundary condition for a range of groundwater table depths (75–600 cm). Panels show 5-day moving averages of the results at the different soil layer depths sampled at the Dahra site (5–100 cm). Model output was interpolated to match the soil sampling depths.

## References


Beck, H. E., Wood, E. F., Pan, M., Fisher, C. K., Miralles, D. G., Dijk, A. I. J. M. van, McVicar, T. R., and Adler, R. F.: MSWEP V2 Global 3-Hourly 0.1° Precipitation: Methodology and Quantitative Assessment, Bulletin of the American Meteorological Society, 100, 473–500, https://doi.org/10.1175/BAMS-D-17-0138.1, 2019.

Campbell, G. S.: A SIMPLE METHOD FOR DETERMINING UNSATURATED CONDUCTIVITY FROM MOISTURE RETENTION DATA, Soil Science, 117, 311, 1974.

Cosby, B. J., Hornberger, G. M., Clapp, R. B., and Ginn, T. R.: A Statistical Exploration of the Relationships of Soil Moisture Characteristics to the Physical Properties of Soils, Water Resources Research, 20, 682–690, https://doi.org/10.1029/WR020i006p00682, 1984.

Gerten, D., Schaphoff, S., Haberlandt, U., Lucht, W., and Sitch, S.: Terrestrial vegetation and water balance - Hydrological evaluation of a dynamic global vegetation model, Journal of Hydrology, 286, 249–270, https://doi.org/10.1016/j.jhydrol.2003.09.029, 2004.

Haxeltine, A. and Prentice, I. C.: BIOME3: An equilibrium terrestrial biosphere model based on ecophysiological constraints, resource availability, and competition among plant functional types, Global Biogeochemical Cycles, 10, 693–709, https://doi.org/10.1029/96GB02344, 1996.

Hengl, T., Heuvelink, G. B. M., Kempen, B., Leenaars, J. G. B., Walsh, M. G., Shepherd, K. D., Sila, A., MacMillan, R. A., De Jesus, J. M., Tamene, L., and Tondoh, J. E.: Mapping soil properties of Africa at 250 m resolution: Random forests significantly improve current predictions, PLoS ONE, 10, 1–26, https://doi.org/10.1371/journal.pone.0125814, 2015.

Ireson, A. M., Spiteri, R. J., Clark, M. P., and Mathias, S. A.: A simple, efficient, mass-conservative approach to solving Richards' equation (openRE, v1.0), Geoscientific Model Development, 16, 659–677, https://doi.org/10.5194/gmd-16-659-2023, 2023.

Kergoat, L.: A model for hydrological equilibrium of leaf area index on a global scale, Journal of Hydrology, 212–213, 268–286, https://doi.org/10.1016/S0022-1694(98)00211-X, 1998.

Monteith, J. L.: Accommodation between transpiring vegetation and the convective boundary layer, Journal of Hydrology, 166, 251–263, https://doi.org/10.1016/0022-1694(94)05086-D, 1995.

Muñoz-Sabater, J., Dutra, E., Agustí-Panareda, A., Albergel, C., Arduini, G., Balsamo, G., Boussetta, S., Choulga, M., Harrigan, S., Hersbach, H., Martens, B., Miralles, D. G., Piles, M., Rodríguez-Fernández, N. J., Zsoter, E., Buontempo, C., and Thépaut, J.-N.: ERA5-Land: a state-of-the-art global reanalysis dataset for land applications, Earth System Science Data, 13, 4349–4383, https://doi.org/10.5194/essd-13-4349-2021, 2021.

Nord, J., Anthoni, P., Gregor, K., Gustafson, A., Hantson, S., Lindeskog, M., Meyer, B., Miller, P., Nieradzik, L., Olin, S., Papastefanou, P., Smith, B., Tang, J., Wårlind, D., and contributors, and past L.-G.: LPJ-GUESS Release v4.1.1 model code, , https://doi.org/10.5281/zenodo.8065737, 2021.

Prentice, I. C., Sykes, M. T., and Cramer, W.: A simulation model for the transient effects of climate change on forest landscapes, Ecological Modelling, 65, 51–70, https://doi.org/10.1016/0304-3800(93)90126-D, 1993.

Romano, N. and Santini, A.: 3.3.3 Field, in: Methods of Soil Analysis, John Wiley & Sons, Ltd, 721–738, https://doi.org/10.2136/sssabookser5.4.c26, 2002.

Rost, S., Gerten, D., Bondeau, A., Lucht, W., Rohwer, J., and Schaphoff, S.: Agricultural green and blue water consumption and its influence on the global water system, Water Resources Research, 44, https://doi.org/10.1029/2007WR006331, 2008.

Sitch, S., Smith, B., Prentice, I. C., Arneth, A., Bondeau, A., Cramer, W., Kaplan, J. O., Levis, S., Lucht, W., Sykes, M. T., Thonicke, K., and Venevsky, S.: Evaluation of ecosystem dynamics, plant geography and terrestrial carbon cycling in the LPJ dynamic global vegetation model, Global Change Biology, 9, 161–185, https://doi.org/10.1046/j.1365-2486.2003.00569.x, 2003.

Verbruggen, W., Schurgers, G., Meunier, F., Verbeeck, H., and Horion, S.: Simulated Tree-Grass Competition in Drylands Is Modulated by CO2 Fertilization, Earth's Future, 12, e2023EF004096, https://doi.org/10.1029/2023EF004096, 2024.

Verbruggen, W., Wårlind, D., Horion, S., Meunier, F., Verbeeck, H., and Schurgers, G.: LPJ-GUESS with soil water movement based on Richard's equation (LPJ-GUESS-RE), , https://doi.org/10.5281/zenodo.15024130, 2025.